PERFORMANCE IMPROVEMENT BY TEMPERATURE CONTROL OF AN OPEN-CATHODE PEM FUEL CELL SYSTEM

S. Strahl[a],*, M. Perrier[b], A. Husar[a], J. Riera[a], M. Serra[a]
[a] IRII (UPC/CSIC) c. Llorens I Artigas 4, 08028 Barcelona, Spain
[b] Ecole Polytéchnique de Montréal, Montréal, Canada
*sstrahl@iri.upc.edu

ABSTRACT
The work presented in this article combines experimental analysis and theoretical studies of temperature effects on the performance of an open-cathode, self-humidified PEM fuel cell system for the design of optimization strategies. The experimental analysis shows the great potential of improving the system performance by proper temperature management. The most significant temperature dependent parameters of the system under study are the activation polarization and the water content of the ionomer of the catalyst layer. An Extremum seeking control algorithm is proposed to regulate the temperature to a voltage maximum. However, the slow dynamics of the temperature related catalyst-drying effect on performance complicate the optimal thermal management via model-free control strategies.

1. INTRODUCTION
PEM fuel cells provide advantages over other fuel cell technologies due to their high power densities and low operating temperatures. The low temperature allows for the use of low cost materials and less severe degradation due to large thermo-cycles. The fuel cell temperature is directly linked to water content in the ionomer of the membrane and the catalyst layers, which is the key factor of PEM fuel cell performance. The resulting restrictions for the thermal management make proper fuel cell temperature control essential in order to maintain proper ionomer humidification and guarantee optimal performance.
Fuel cell system modeling has played a decisive role in developing, optimizing and testing of fuel cell control strategies. However, modeling and controlling PEM fuel cell based systems is a particularly challenging task due to the interactions between physical phenomena of different nature and the presence of nonlinear structures [1]. The work presented by [2] shows a first approach of how to control temperature of PEM fuel cells. However, optimal thermal management related to humidification is still a crucial issue in every PEM fuel cell based system.
This work presents an experimental analysis of temperature effects in an open-cathode, self-humidified PEM fuel cell system and the resulting dynamic temperature and voltage models. Finally, simulation and experimental results are used to discuss possible control strategies for performance improvement via proper temperature control.

2. EXPERIMENTAL ANALYSIS

2.1 Experimental setup
The system under observation in this work is the commercially available 100W, 20 cell PEM fuel cell stack H-100 from Horizon Fuel Cells Technologies. This open-cathode system with an active area of 22.5cm^2 is self-humidified and air-cooled. It includes a cooling fan directly attached to the fuel cell housing, which removes heat from the stack by forced convection and at the same time provides oxygen to the cathode. The anode inlet is supplied with dry hydrogen and the outlet features a normally-closed electromagnetic valve for dead-ended operation and purging. For testing the stack is installed in an environmental chamber to be able to control the ambient conditions (relative humidity, temperature and oxygen concentration).

2.2 Flow rate and temperature mapping
In order to check the applicability of performance optimization techniques via temperature control, the steady-state input-output transfer characteristics of the fuel cell system were identified experimentally. The input of the system is the PWM duty cycle of the cathode cooling fan, and the output is the stack voltage. The characteristic curves of stationary operation points were recorded in the linear region of the polarization curve for current densities form 0.09 to 0.27 Acm^{-2}, as shown in Figure 1(a). Figure 1(b) shows the same experiment only with the difference of selecting the stack temperature as the x-coordinate, which is directly influenced by the fan flow rate. The ambient temperature and relative humidity are kept constant by the environmental chamber (T_{amb}=25ºC, RH_{amb}=75%). The stack current was set by a programmable load and the

PWM duty cycle was modified from high to low. The operating range of the fan is limited from 50% to 100% duty cycle due to the detent torque of the fan. Lower duty cycles would lead to stalling of the fan. The minimum flow rate at 50% duty cycle still guarantees a cathode stoichiometry of 20. Thus, the stoichiometric effect of changes in the flow rate is negligible, whereas the effect on performance is caused by the change in the stack temperature, plotted in Figure 1(b).

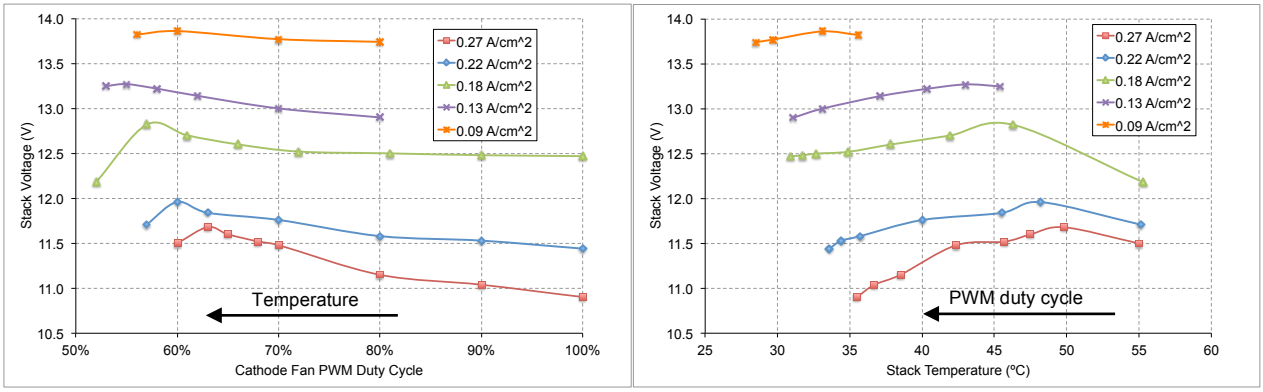

(a) (b)

Figure 1. PWM duty cycle (a) and stack temperature (b) mapping against stack voltage

The curves in Figure 1 clearly show that a voltage maximum exists at each current density at low cathode flow rates. Especially at the higher current densities a significant system performance gain can be obtained by optimal temperature control, compared to the system's standard controller, which tries to maintain the stack temperature between 35 and 45 ºC at standard operating conditions. For instance, at 0.18 Acm^{-2} a stack power gain of 2% is reached by increasing the temperature from the standard setpoint of 39 to 46 ºC. In turn, the power consumption of the fan is reduced by 14%, which equals 2% of the stack power at this operation point. Thus, the total performance improvement of the system by optimizing the temperature setpoint is 4% of the stack power.

As shown in Figure 1(b), a further increase in temperature beyond the voltage maximum leads to a severe voltage loss. This is caused by drying of the catalyst layer, since the electrolyte material in the catalyst layer requires the presence of water for the H+ ions to reach the so-called three-phase-contacts between reactant gas, electrolyte, and electrode catalyst [3].

The dynamics of this phenomenon at 0.18 Acm^{-2} are shown in Figure 2. In this experiment the PWM duty cycle was decreased stepwise from 62% to 51% and increased afterwards back to 64%, as depicted in Figure 3(a). As stated above, the voltage increases with increasing temperature. However, at about 50ºC the characteristic voltage response changes. Even though the voltage still increases at the beginning of a step, it does not stabilize but keeps decreasing with time due to the drying effect. Increasing the temperature even more leads to a more severe voltage decline rate, as shown in Figure 2(a). These unstable points are marked in red in Figure 3, whereas the assumed stationary points where the voltage could stabilize are marked in green. From the control point of view the unstable region represents a challenging problem, since after a change in the control action the fuel cell reacts positively, which means a performance improve can be detected. However, no stationary points are reached since the voltage keeps dropping and the actual performance is worse than at the initial conditions.

Decreasing the temperature stepwise afterwards leads to a similar characteristic voltage response, as depicted in Figure 2(b). The overall voltage trend is positive and leads to an improved performance, however at the beginning of a step in the duty cycle the voltage first drops and then recovers. The reason is that at a very dry state of the cathode catalyst layer a step in the PWM duty cycle towards higher cathode air flow rates increases the water removal rate from the cathode. However, the cooling effect of the higher flow rate, which is slower than the water removal effect, allows for a higher water content in the catalyst layer. Thus, the steady-state performance increases. At higher flow rates (lower temperatures) this effect disappears, because the system is well humidified and therefore temperature related effects overbalance water removal effects.

Figure 3 shows the trajectory of the stack voltage as a function of PWM duty cycle and stack temperature. The plots depict that the system shows hysteresis, but the maximum exists in both directions and is located at the same PWM duty cycle setpoint.

Finally, the experimental analysis shows a major drawback for optimization strategies, which are the slow dynamics of the system. As depicted in Figure 2, the time constant of the voltage response after a step in

PWM duty cycle is between 2 and 3min, depending on the operation point. However, for reaching steady-state it may take more than 30min. Moreover, after passing the maximum the system becomes unstable and the voltage keeps decreasing linearly within the allowed operating range while the temperature increases due to the loss of efficiency.

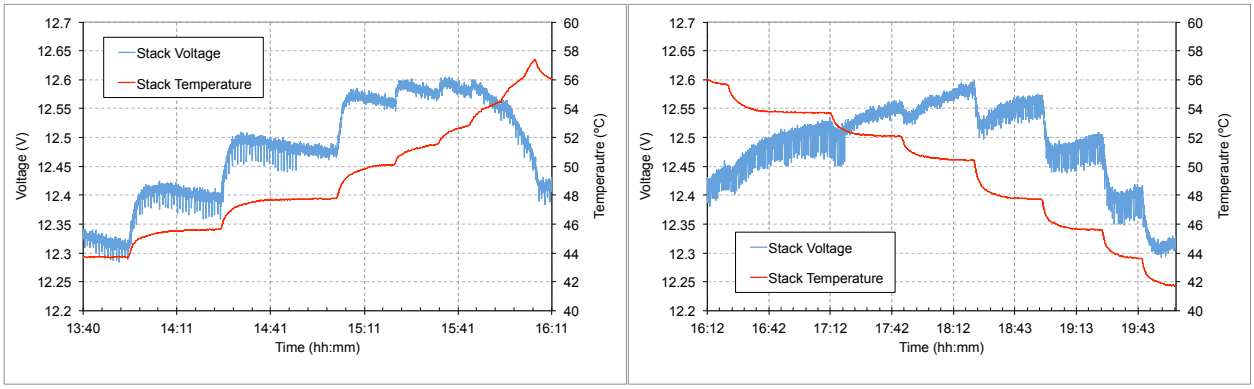

(a) (b)

Figure 2. Stack temperature and voltage over time during down-stepping (a) and up-stepping (b) of fan PWM duty cycle at 0.18 Acm^{-2}

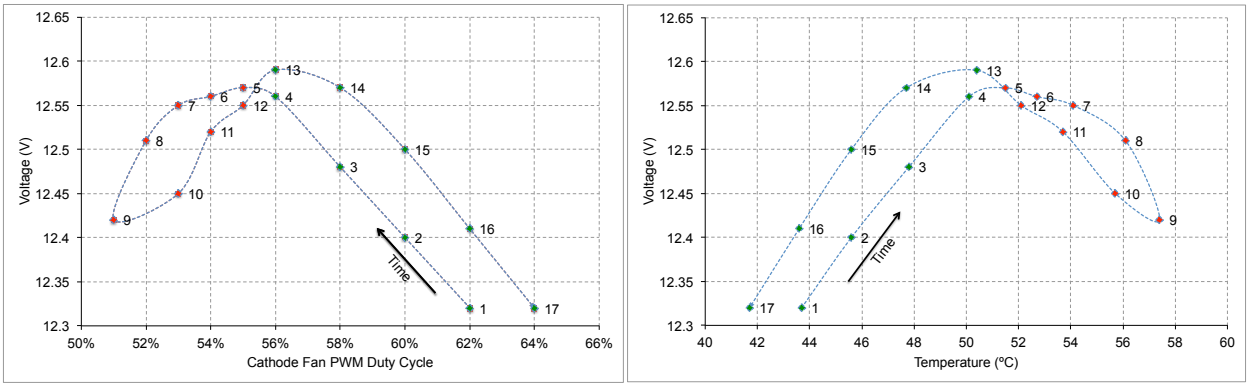

(a) (b)

Figure 3. Stack voltage trajectory as a function PWM duty cycle (a) and stack temperature (b) at 0.18 Acm^{-2}. Stable points are marked in green, unstable point in red

3. MODELING AND CONTROL APPROACH

This approach tries to describe the presented experimental results mathematically in order to develop control strategies for optimal temperature management and performance improvement.

3.1 Thermal model

Regarding the fuel cell stack as a heated solid block, the total heat transfer rate can be expressed as:

$$\frac{dQ_{fc}}{dt} = m_{fc} C_{p,fc} \frac{dT_{fc}}{dt} = \dot{Q}_{tot} - \dot{Q}_{cool} - \dot{Q}_{loss} \quad [W] \tag{1}$$

The stack's mass m_{fc} and specific heat capacity $C_{p,fc}$ have been determined experimentally, as published earlier in [4]. Since the stack is air cooled, heat is removed by forced and natural convection. Thus, the overall heat transfer rate can be described by the sum of the heat sources and sinks. The second right hand side of equation (1) represents the total rate of heat generation minus the heat removal rate by forced convection and the uncontrolled heat loss due to natural convection from the fuel cell surface to the surroundings, as described in detail in [4]. Similar to [5] the heat loss to the environment is assumed to be 10 % of the total waste heat in this work. The total rate of heat generation is a function of the electrical power P_{el} drawn from the system and the stack's efficiency at the respective operation point $\eta_{LHV,stack}$, as

described by equation (2). Hence, the temperature change of the stack over time as a function of generated and removed heat can be described with the following set of equations:

$$\dot{Q}_{tot} = P_{el}\left(\frac{1}{\eta_{LHV,stack}} - 1\right) \quad [W] \tag{2}$$

$$\dot{Q}_{cool} = \rho_{air} A_{inlet} v_{air} C_{p,air}\left(T_{fc} - T_{amb}\right) \quad [W] \tag{3}$$

$$\frac{dT_{fc}}{dt} = \frac{1}{m_{fc} C_{p,fc}}\left(0.9\dot{Q}_{tot} - \dot{Q}_{cool}\right) \quad [K\,s^{-1}] \tag{4}$$

Equation (3) describes the heat removal by the cooling fan as a function of the ambient air density ρ_{air}, temperature T_{amb}, heat capacity $C_{p,air}$, inlet velocity v_{air} and cross-sectional inlet area A_{inlet}. The dynamic of the fan is modeled by a first-order linear time-invariant (LTI) system with T=1s in combination with a transport delay of 1s. The gain of the system, which relates the PWM set point to the cathode inlet velocity is modeled by a third order polynomial, according to the experimental data. The model was validated against experimental data from laboratory tests with the studied fuel cell stack.

Regarding the thermal model in the state space representation, the only state x of this system is the fuel cell temperature T_{fc}. The load current I, the electrical power output P_{el} and the cathode inlet air temperature T_{amb} can be considered as a perturbations. The control action u of the system is the PWM duty cycle of the cathode fan, which sets the inlet air velocity v_{air}. Thus, the state equation of the thermal model results in:

$$\dot{x}(t) = K_z Z(t) + k_u x(t) u(t) + k_u u(t)\begin{bmatrix} 0 & 0 & 1 \end{bmatrix} Z(t) \tag{5}$$

where:

$$Z(t) = \begin{bmatrix} I(t) & P_{el}(t) & T_{amb}(t) \end{bmatrix}^T, \quad K_z = \begin{bmatrix} \frac{0.9 \cdot 1.254 \cdot n_{cell}}{m_{fc} \cdot C_{p,fc}} & \frac{-0.9}{m_{fc} \cdot C_{p,fc}} & 0 \end{bmatrix}, \quad k_u = \frac{\rho_{air} \cdot A_{inlet} \cdot C_{p,air}}{m_{fc} \cdot C_{p,fc}} \tag{6}$$

The state equation (5) shows that the system is non-linear, because the control action is multiplied by the state variable, however control-affine in a certain range of operating conditions. Thus, a simple proportional-integral (PI) controller is proposed for the temperature control task.

3.2 Temperature controller

The PI controller has been designed following the tuning rules of Ziegler and Nichols in the frequency domain [6]. The control law is shown in equation (7). The offset *e(t)* is the difference of the temperature setpoint and the measured stack temperature. The applied proportional gain k_p is 0.8 and the integrator time constant T_i is 20.

$$u(t) = k_p e(t) + \frac{1}{T_i}\int_0^t e(\tau)\, d\tau \tag{7}$$

As explained above, the temperature is controlled via a cooling fan, which is a DC electronic motor with a voltage limit. This limit is represented in the model by an actuator saturation above 100 % PWM and below 50% PWM. When the control action excesses this limit, the feedback loop is broken and the system runs in open loop because the actuator remains saturated. In order to avoid a building up of the integral term, an anti-windup loop has to be integrated into the controller. The controller was implemented in Simulink and tested in combination with the developed thermal model of the fuel cell under different operating conditions, perturbations and set points. Experimental polarization curve data was included in order to determine the stack voltage at the respective current setpoint. Figure 2 shows the performance of the temperature controller during a dynamic test period of 1000s. Band-limited noise based on experimental data is added to the temperature feedback of the simulation in order to account for measurement noise. The designed PI controller manages to control the temperature fast and properly, as shown by Figure 4.

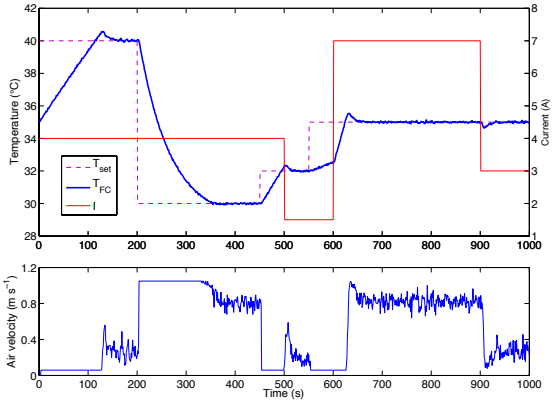

Figure 4. Temperature controller simulation results

3.3 Voltage model

The cell voltage of a PEM fuel cell V_{fc} can be described as the thermodynamic reversible potential E_{th} minus the three major voltage losses: activation polarization η_{act}, ohmic η_{ohm} and mass transport η_{mt}.

$$V_{fc} = E_{th} - \eta_{act} - \eta_{ohm} - \eta_{mt} \quad [V] \tag{8}$$

Since every component of equation (8) is dependent on temperature, the effects have to be seperated in order to describe the phenomena observed in the experiments.

The thermodynamic reversible potential is defined by the Nernst equation as a function of Gibbs free energy, temperature and pressure and decreases linearly with temperature [7]. However, in the operating range of the system under study between 30 and 60 ºC this temperature effect is negligible.

The mass transport losses decrease with increasing temperature since the limiting current density is a function of the reactant diffusivity, which in turn is a strong function of temperature [7]. The temperature related phenomena shown in chapter 2 are all observed in the linear region of the polarization curve at current densities much smaller than the limiting current density. Hence, the temperature dependency of the mass transport losses does not affect the voltage response under these specific conditions. Possible changes in the concentration gradient along the reactant flow channels have been compensated by operating at high reactant stoichiometries ($\upsilon_{an} > 2$, $\upsilon_{cat} > 20$).

The ohmic losses depend on the ionic conductivity of the membrane, which increases linearly with increasing water content and exponentially with temperature [8]. Temperature and water content are strongly related since the membrane water content depends on the water saturation pressure, which in turn is a function of temperature. Hence, there is a tradeoff between increasing temperature and water content in order to optimize ionic conductivity. However, as shown in experiments of [9] and [10], the change in the ohmic losses due to temperature is only responsible for a relatively small part of the voltage increase/decay, shown in chapter 2. The major part is related to changes in the activation polarization losses. Equation (9) describes these losses using a Tafel approach [7]:

$$\eta_{act} = \frac{RT}{\alpha n F} \ln\left(\frac{i}{i_0}\right) \quad [V] \tag{9}$$

The activation polarization losses feature two different temperature dependencies. On one hand, as shown in equation (10), these losses increase linearly with temperature, but on the other hand, the exchange current density i_0 increases exponentially with temperature, as described by equation (10). The physical reason for this effect is the increasing available thermal energy in the system, which increases the likelihood that a given reactant will possess sufficient energy to reach the activated state [7].

$$i_0 \propto e^{\frac{-\Delta G^*}{RT}} \tag{10}$$

Thus, a performance improvement due to a reduction in activation polarization losses by increasing temperature is guaranteed if equation (11) is valid:

$$\eta_{act} < \frac{\Delta G^*}{\alpha n F} \tag{11}$$

Assuming a constant activation barrier ΔG^* of 66 kJmol^{-1} for oxygen reduction on platinum [11], this criteria is always fulfilled in the specific operating range of the studied fuel cell stack, as shown by the experimental data for activation polarization obtained by [10].
In conclusion, the improved reaction kinetics through a higher exchange current density are responsible for the majority of the voltage gain obtained by increasing the temperature. For instance, a positive temperature step of 2 ºC, as depicted in Figure 2, results in a theoretical stack voltage gain of 86 mV only due to the increase of i_0 by 17%. However, the capability of improving performance by increasing temperature is limited due to drying of the cathode catalyst layer by elevated temperatures and the related loss of active sites [9], as shown in the experiment. Moreover, the dynamic of the temperature related drying effect on fuel cell voltage is very slow and strongly dependent on the operating conditions. Hence, in order to obtain a complete and valid voltage model of the fuel cell, the mesoscopic effects, such as hydration and dehydration effects of the catalyst layer, as described similarly by [12] and [13] have to be taken into account. However, such a multiscale modeling approach is out of the scope of this work. Instead, a simple mathematical model, obtained by parameter fitting with experimental data, is used in order to design an Extremum seeking controller, since this controller type does not require a model of the plant. Equation (12) presents the transfer function of the second order dynamic model between the PWM duty cycle of the cathode fan and the stack voltage of the fuel cell.

$$\frac{Y(s)}{U(s)} = \frac{K_u(i)}{120s+1} - \frac{0.1}{600s+1} \tag{12}$$

The first term on the right hand side of equation (12) represents the voltage response due to the change in temperature. The gain $K_u(I)$ is defined by the PWM duty cycle mapping against stack voltage as a function of current density, as presented in Figure 1(a). The second term on the right hand side represents the temperature related catalyst drying effect with a 5 times slower time constant and a fixed gain. The nonminimum phase effect ("wrong way effect"), as observed in Figure 2(b) when decreasing the temperature, is not considered in this model since the effect only occurs in the unstable region of Figure 3. Steady operation in this region has to be avoided to prevent excessive drying.
Figure 5 shows the experimental validation of the model using the experimental data shown in Figure 2(a) after a decrease in the PWM duty cycle from 60 to 58%. The modeled dynamic of the catalyst drying effect coincides well with the experiment.

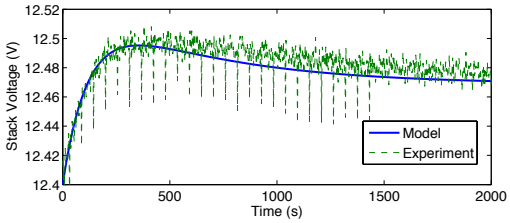

Figure 5. Voltage model validation

3.4 Extremum seeking control for performance optimization

As explained in the previous section, an accurate voltage model that could be used in adaptive control strategies for regulation to predicted setpoints is difficult to obtain. Thus, a self-optimizing control algorithm is applied in this work in order to maximize the voltage output of the fuel cell by adaption of a previously unknown reference point. The main advantage of this technique is that no knowledge about the plant is required, since the regulation is based on the input-output behavior of the system only. Figure 6 shows the control scheme, similar to the published work of [14]. The major difference is that cascade control is used in this work. Hence, the temperature is controlled by the PI controller, described in section 3.2, while the Extremum seeking algorithm calculates the temperature setpoints. Since the wind-up problem is solved in the temperature control loop it does not affect the integrator of the Extremum seeking loop. The basic idea of the Extremum seeking algorithm is to move the system around the neighborhood on both sides of a maximum by application of a slow periodic perturbation and analyzing the system's response [14]. The estimated gradient determines the sign and gain adaption of the control action. Thus, optimization is achieved by regulating the norm of the gradient at zero [15]. The main problem of this technique is that the perturbation frequency should be slow enough to consider the system to be static [15]. This, however, may result in convergence rates much slower than the system dynamics. Since the time constant of the system is around 120s, depending on the operating conditions, the perturbation frequency was set to 0.008Hz.

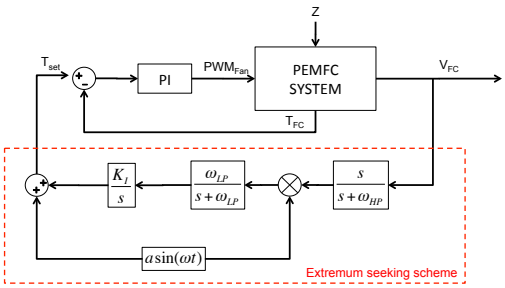

Figure 6. Control scheme

The controller was implemented, adjusted and tested in Matlab/Simulink. Figure 7 shows the simulation results at an operation point of 0.18 Acm^{-2}. Band-limited noise based on experimental data is added to both the temperature and the voltage feedback of the simulation in order to account for measurement noise. The cut-off frequencies of the High-Pass filter ω_{HP} and the Low-Pass filter ω_{LP} were adjusted to 0.002 rad^{-1} and 0.01 rad^{-1}, respectively. The amplitude a of the perturbation signal was set to 0.3 ºC and the integrator gain K_I was adjusted to 0.015. The simulation shows that the algorithm is capable of finding the maximum within about 15min and keeping the voltage at that point. At the beginning of the simulation the actuator saturates at the lower limit in order to heat up the fuel cell to the optimal temperature. Afterwards the PI controller regulates the stack temperature to the reference provided by the Extremum seeking controller. The system converges after about 20min.

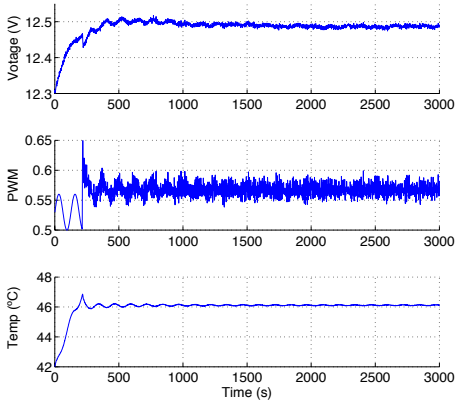

Figure 7. Simulation results at a current density of 0.18 Acm^{-2}

4. IMPLEMENTATION AND TEST

From the Simulink model a Dynamic-link library (DLL) of the controller was created using the Matlab Real-time workshop and implemented into the LabView data acquisition system of the test station. Tests with the controller were performed under the same operating conditions as the characterization experiments, presented in chapter 2. Figure 8 shows the experimental results of the operation with the designed controller at a current density of 0.18 Acm^{-2}. Even though the maximum is reached, the controller does not manage to keep the system at this maximum voltage because of the very slow catalyst drying effect, which complicates the detection of a significant change in the gradient. Decreasing the frequency of the perturbation signal and readjusting the filters might solve this problem, however, this would make the system even slower. A bigger integrator gain could help as well, however this would cause a higher overshoot. Since the system dynamics are slow it would take even more time reach steady-state. The greatest problem is still the slow accommodation of the voltage at a stationary operation point, even if the temperature is well controlled.

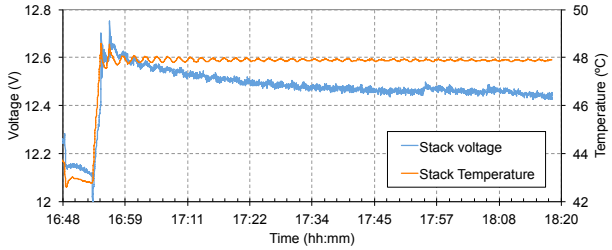

Figure 8. Experimental results at a current density of 0.18 Acm^{-2}

5. CONCLUSIONS

The experimental and theoretical analysis of temperature effects on system performance presented in this work shows the great importance of proper thermal management strategies. The temperature dependency of the exchange current density shows the most significant effect on the performance of the studied open-cathode fuel cell stack. However, the improvement by increasing temperature is limited due to the drying of the ionomer in the catalyst layer at elevated temperatures and the related loss of active sites.

The simulation results with the presented thermal and performance models under operation with the designed Extremum seeking controller show promising results in terms of optimal temperature control. However, the experimental validation resulted in insufficient capability of the controller to stabilize the voltage at the detected maximum. This is a result of the slow system dynamics, especially the gradual voltage decay due to the temperature related drying of the catalyst layer. A possible solution for this problem is the use of a model-based controller in conjunction with a control-oriented model of the fuel cell system that accounts for the explained drying effect. Work is in progress in order to upgrade the model for this purpose.

6. ACKNOWLEDGEMENTS

The experimental work was performed at the Fuel Cells Laboratory of the Institut de Robòtica i Informàtica Industrial (CSIC-UPC, Barcelona). All experiments were only possible due to the laboratories' advanced equipment and proficient technical staff. This work is partially funded by the national project MICINN DPI2011-25649, and by the contract PUMA-MIND FP7 303419 with the European Comission.

REFERENCES

1. C. Kunusch, P. Puleston, M. Mayosky, A. Husar. (2011). Control-Oriented Modeling and Experimental Validation of a PEMFC Generation System. IEEE Transactions on Energy Conversion, 26(3) 851–861.
2. Riascos, L. and Pereira, D. D. (2009). Optimal temperature control in PEM fuel cells. In Industrial Electronics. IECON'09. 35th Annual Conference of IEEE, 2778-2783.
3. James Larminie and Andrew Dicks. (2003). Fuel cell systems explained. John Wiley & Sons, Inc.
4. S. Strahl, A. Husar and M. Serra. (2011). Development and experimental validation of a dynamic thermal and water distribution model of an open cathode proton exchange membrane fuel cell. Journal of Power Sources, 196(9), 4251–4263.
5. E. A. Müller and A. G. Stefanopoulou. (2005). Analysis, modeling, and validation for the thermal dynamics of a polymer electrolyte membrane fuel cell system. Excerpt from the third International Conference on Fuel Cell Science, Engineering and Technology, Ypsilanti, Michigan, USA, no. FUELCELL2005- 74050.
6. Karl Johan Aström and Richard M. Murray. (2008). Feedback systems: An introduction for scientists and engineers. Princton University Press.
7. R. O'Hayre, S. Cha, W. Colella and F. B. Prinz. (2009) Fuel cell fundamentals. John Wiley & Sons, Inc.
8. T. E. Springer, T. A. Zawodzinski and S. Goftesfeld. (1991). Polymer Electrolyte Fuel Cell Model. Journal of The Electrochemical Society, vol. 138, pages 2334–2342.
9. Ciureanu, M. (2004). Effects of Nafion dehydration in PEM fuel cells. Journal of Applied Electrochemistry, 34, 705-714.
10. A. Husar, S. Strahl and J. Riera. (2012). Experimental characterization methodology for the identification of voltage losses of PEMFC: Applied to an open cathode stack. International Journal of Hydrogen Energy, 37(8), 7309-7315.
11. Frano Barbir. (2005). Pem fuel cells: Theory and practice. Elsevier Academic Press.
12. Ohma, A., Mashio, T., Sato, K., Iden, H., Ono, Y., Sakai, K., Akizuki, K. (2011). Analysis of proton exchange membrane fuel cell catalyst layers for reduction of platinum loading at Nissan. Electrochimica Acta, 56(28), 10832-10841.
13. Das, P. K., Li, X., Liu, Z.-S. (2010). Analysis of liquid water transport in cathode catalyst layer of PEM fuel cells. International Journal of Hydrogen Energy, 35(6), 2403-2416.
14. Krstic, M. and Wang, H. (1997). Design and Stability Analysis of Extremum Seeking Feedback for General Nonlinear Systems. Proceedings of the 36th Conference on Decisicion & Control San Diego, California USA, 1743-1748.
15. Chioua, M., Srinivasan, B., Guay, M., Perrier, M. (2007). Solution of Perturbation-Based Extremum Seeking Methods on the Excitation Frequency. The Canadian Journal of Chemical Engineering, vol. 85, 447-453.